Soft X-ray Emission from Post-Pulse Expanding Laser-Produced Plasmas

By

J. L. Weaver[1], U. Feldman[2,3], A. N. Mostovych[1],

J. F. Seely[3], D. Colombant[1], G. Holland[4]

[1] Plasma Physics Division, Naval Research Laboratory, Washington, DC 20375

[2]Artep, Inc., Columbia, MD 21045

[3] Space Science Division, Naval Research Laboratory, Washington, DC 20375

[4] SFA, Inc., 1401 McCormick Drive, Landover, MD 20785

Abstract

A new diagnostic spectrometer has been developed at the Naval Research Laboratory (NRL) to measure the time resolved absolute intensity of radiation emitted by the Nike laser irradiated targets. The spectrometer consists of a dispersive transmission grating of 2500 lines/mm or 5000 lines/mm and a detection system consisting of an absolutely calibrated Si photodiode array and a CCD camera. In this paper, this spectrometer was used to study the spatial distribution of soft x-ray radiation from low Z elements (primarily carbon) that lasted tens of nanoseconds after the main laser illumination was over. Using the newly developed spectrometer, we recorded soft x-ray emission as a function of the target material and target orientation with respect to the incoming laser beam and the spectrometer line of sight. While a number of spectral features have been identified in the data, the instrument's combined temporal and spatial resolution led to the observation of the plasma expansion from CH targets for up to ~ 25 ns after the cessation of the main laser pulse. The inferred plasma expansion velocities are slightly higher than those previously reported.

I. Introduction

Planar solid targets irradiated by high intensity, short duration laser pulses (~10 ns or less) have been studied since the late 1960's [1-8]. These early studies found that irradiation by the laser created a plume of plasma that expanded from the surface of the target with typical ion velocities on the order of 10^7 cm/s. They also established the fact that highly ionized atoms can persist for tens of nanoseconds after the cessation of the laser pulse. This 'frozen ionization' of the laser-produced plasma resulted in emission arising many millimeters from the initial target surface. For these early experiments, near-UV and visible spectral lines were typically chosen for quantitative, time-resolved studies of the plasma dynamics. Although some observations were made in the EUV/soft x-ray region, time resolution and absolute intensity calibration were not typically achieved in this wavelength region. The main point for this paper is to present new spatially resolved observations from a transmission grating spectrometer during the post pulse plasma.

The Nike laser program the Naval Research Laboratory (NRL) has been interested in measurements of soft x-rays (0.1-1.0 keV) to explore radiation effects - e.g. non-local thermodynamic equilibrium (NLTE) opacities of high-Z targets and radiation transport - relevant to direct drive inertial confinement fusion [9,10]. The primary instrumental requirements were modest spectral and temporal resolution and accurate absolute intensity calibration. An optical system that provides a flat focal field at the detection plane was desired mainly to allow the use of a variety of standard time-resolving detectors (streak camera, microchannel plate, photodiode arrays) and such systems also allow for the possibility of spatial resolution as used in this paper.

Transmission gratings and concave variable line space gratings are two of the most commonly used diffraction elements for such spectrometers [11-20]. They both can be selected to cover the required spectral region with similar spectral resolution at the detector plane ($\delta\lambda/\delta x \sim 1.0$ Å/mm). Although concave variable line space gratings provide a means to collect and focus the photons onto the detector, transmission gratings have a greater advantage in the fact that they can be used at normal incidence. This arrangement is much simpler to align and maintain, particularly in regard to the absolute calibration: a grazing incidence system will be more sensitive to the accumulation of contaminants than a normal incidence system. In addition to the choice of a transmission grating, the need for robust absolute calibrations also led to the choice of a Si photodiode array for the primary detection element.

In a series of experiments, emission was observed from planar targets made of BN, CH, Kapton, Al, W and Au. During the main pulse, the transmission grating spectrometer provided a spatially integrated measurement of the time history of the soft x-ray emission originating in the region of the laser focus close to the target surface but after the laser pulse, a late time peak in the emission was observed for the CH targets from regions far from the initial target surface. Unlike earlier investigations [1-8], this paper presents an absolutely calibrated observation of the post pulse plasma expansion with simultaneous spatial, temporal, and spectral resolution. A brief description of the transmission grating spectrometer and the experimental procedures are given in Section II. In Section III, the optical properties of the spectrometer are discussed. Section IV presents the time resolved spectra from the various materials used for planar targets. Section V discusses the expanding CH plasma.

II. Experimental Procedure

The spectrometer is comprised of two distinct modules coaligned along the line of sight, Fig. 1. The front module consists of a rectangular entrance slit (0.060 mm x 7.62 mm) followed by a transmission filter (free-standing 2600 Å Ti or 1600 Å Al foil) and a gold transmission grating with either 2500 lines/mm or 5000 lines/mm. The entrance slit is oriented such that its long dimension is parallel to the grating bars. The slit and filter were placed in front of the grating to shield it from possible damage by radiation and debris originating at the target. The rear module houses the spectrometer detection system: a set of Si photodiodes and a charge-coupled device (CCD) array. The transmission of the filters, the responsivity of the Si photodiodes, and the diffraction efficiency of the first four orders of the diffraction grating have been measured as a function of incident wavelength at the National Synchrotron Light Source at Brookhaven National Laboratory [20]. The transmission grating calibration demonstrated that the second order diffraction efficiency was only ~10% that of the first order.

The CCD camera records a time-integrated spectrum of the target emission. Because the CCD's sensitivity to soft x-ray radiation is fairly low, a phosphor scintillation screen (gadolinium oxysulfide doped with terbium) is placed over the CCD to convert the soft x-rays into visible light that is more efficiently detected by the CCD. A ten element Si photodiode array is placed just in front of the CCD. Each element is 1.014 mm wide and 1.014 mm tall and is separated from its neighbor by a 0.054 mm wide gap. A tall rectangular entrance slit (60 μm wide) allows light to fall simultaneously on the Si photodiode array and the CCD array. A mask with apertures has been placed in front of the photodiode array. The apertures are designed to limit the

exposed area of each Si photodiode to a width of 0.818 mm and to cast a pattern of shadows on the CCD image that is precisely aligned to the diode positions. Comparison of the location of the shadows and the location of the recorded spectral features is used to determine the wavelength range of the radiation absorbed by each of the Si diodes to within 1-2 pixels or about 12% of the aperture width. The output of the Si photodiodes is connected to a bias circuit that includes a 1 GHz band pass oscilloscope providing a temporal resolution better than 1 ns.

The spectroscopic studies have been made using planar targets irradiated by three to ten beams of the Nike laser at NRL [20]. The transmission grating spectrometer was installed on a port that had an angle of 42° from the target normal and the spectrometer's entrance slit rested primarily in the horizontal plane. The laser pulse had a ~4 ns duration and yielded energies between 20 and 40 J per beam. The full width half maximum (FWHM) of the focal spot on target ranged from 750 μm to 1500 μm. The prepulse intensities during our observations were typically less than 2 % of the main pulse intensity. The peak laser irradiance on target ranged from $3x10^{11}$ to $2x10^{13}$ Wcm^{-2}.

III. Optical Properties of Transmission Grating Spectrometer

The spectrometer essentially operates as a 1-D pinhole camera with moderate spatial resolution in the direction perpendicular to the entrance slit and poor spatial resolution in the direction parallel to the entrance slit. The spectrometer collects radiation over a rectangular slice through the target region with a narrow width in the direction perpendicular to the slit and an elongated height in the direction parallel to the slit. For the given positions of the target, entrance slit, and Si photodiode array, the height of a photodiode's collection region can be estimated. In the experiment, the source-slit

distance was approximately 1.21 m, the slit-detector distance was approximately 0.69 m, and the entrance slit had a height of 7.62 mm. The 1.014 mm height of the diodes translates to a 15.1 mm long region near the target. The narrow dimension of the collection region can be estimated from the ~0.82 mm width of the diode mask, the source-slit distance, and the slit-detector distance:

$$\delta x \approx 0.82\ \text{mm}\,\frac{1.21\ \text{m}}{0.69\ \text{m}} \approx 1.44\ \ \text{mm} \qquad (1).$$

The separation between the collection regions of adjacent diodes is calculated the same way (with 1.07 mm in place of 0.82 mm) and has a value of 1.88 mm. In most experiments, due largely to the 42° viewing angle of the spectrometer, the collection region will not be aligned either parallel or perpendicular to the target normal. The elongated axis of the collection region will have a projection parallel to the normal as well as perpendicular to the target normal. The estimate of spatial resolution requires a further division by sinθ or cosθ for the distance parallel or perpendicular to the target normal, respectively.

A complicating factor to this description is the presence of the transmission grating close to the entrance slit. Radiation that enters the spectrometer's slit is dispersed by the parallel bars of the transmission grating according to the equation:

$$m\lambda = d\left(\sin\theta + \sin\theta_i\right) \qquad (2)$$

where λ is the radiation wavelength, d is the grating period, m is the diffraction order, θ is the diffraction angle, and θ_i is the angle of incidence of the emission on the grating. Note that both angles are small in these experiments (less than 0.5^{o}). This diffraction occurs in the direction perpendicular to the bars of the transmission grating, which, in this paper, have been aligned parallel to the long dimension of the entrance slit. The pattern

created by the grating consists of an undispersed image of the emission region corresponding to the m=0 (zero order) solution of Eq. 1 and multiple images to either side that correspond to the various higher diffraction orders (integer values where $m \neq 0$) of the wavelength dependent emission. From Eq. 2, at a fixed value of wavelength, we can see that any increase or decrease in the angle of incidence will correspond to an equal and opposite change in the diffraction angle. When the emission region moves along the dispersion direction (i.e. the spatially resolving direction perpendicular to the long dimension of the entrance slit), zero order and all other spectral features move in the opposite direction in the detection plane. For the work described in this paper, the diffraction angle is sufficiently small that the value of $\sin\theta$ can be accurately approximated by θ. The plate factor ($\delta\lambda/\delta x$) at near-normal incidence ($\theta_i \sim 90^o$) is then expressed as a simple constant for each diffraction order (m):

$$\frac{\delta\lambda}{\delta x} \approx \frac{d}{mD} \qquad (3)$$

where x is the distance along the direction of the dispersion at the surface of the CCD and D is the distance between the grating and the detector. Consequently, the separation distance between the zero order and the higher order spectral features at the detection plane remains unchanged as the emission position moves over small distances near the target.

Due to the interrelated effects of spatial motion and spectral dispersion, interpretation of the spectrometer data in Section IV will have to consider the spectral resolution provided by the grating. For a fixed geometrical arrangement, the expected

instrumental width – full width at half maximum (FWHM) - of a transmission grating spectrometer can be estimated from a simple formula:

$$\Delta\lambda \approx \frac{d(S+W_s)}{R} + \frac{dW_s}{D} \qquad (4)$$

where S is the diameter of the source, R is the distance from the source to the entrance slit, D is the distance from the entrance slit to the detector, W_s is the width of the entrance slit, and d is the distance between the bars of the transmission grating. In our experiments, the source-grating and grating-detector distances were R = 1.21 m, and D = 0.69 m and the entrance slit width was 0.060 mm. The instrumental resolution (FWHM) at the CCD and Si diodes in the case of the 2500 lines/mm (4000 Å /period) was ~ 3.03 Å when the nominal laser spot diameter was S=750 μm. For the same arrangement, the plate factor indicates that each diode (masked by a 0.818 mm wide aperture) covered a spectral range of ~4.7 Å with the gaps between Si photodiodes corresponding to 0.9 Å. Although each diode collects light over a wavelength range slightly larger than the instrumental width of the spectrometer, the separation between diodes could permit a slight overlap of emission at a single wavelength.

IV. Time resolved spectra from planar targets

In our experiments we used three types of targets made of low Z, moderate Z and high Z elements (where Z is the atomic number of the element). The targets in the low Z category were made of CH, BN and Kapton while as a representative for the moderate Z targets we used Al. When using targets made from the low Z elements only the 1s-2ℓ (for ℓ>1) type transitions appear in the spectrometer's spectral range. In the case of CH targets it implies that only lines of C V and C VI and their free bound continuum appear. For high Z targets we used solid Au and W foils.

IV.1 High Z targets: Figure 2 shows the time history of the photodiode signals for a planar Au target that was irradiated with 3 Nike beams (laser power density of ~$5x10^{12}$ Wcm^{-2}). In Fig. 2, the recorded flux from the photodiodes is compared to the normalized intensity of the laser pulse, shown in the last position on the graph. The emission from the Au target follows the laser time history to within the resolution of the Si photodiodes (~1 ns). An identical result is obtained when W targets rather than Au targets are used. This result confirms a well-known fact for Nike illuminated targets: the ionization and recombination processes for high Z elements are very rapid. The high Z targets demonstrate the subnanosecond time resolution of the transmission grating spectrometer.

IV.2 Low Z targets

CH Targets: Figure 3a shows the photodiode signals for a planar CH target that was irradiated with 10 Nike beams (laser power density of ~$2x10^{13}$ Wcm^{-2}). The largest signal is obtained for the diode aligned to the Lyman-α (Lyα) line of hydrogen-like carbon at 33.7 Å (i.e. the diode centered 32.5 Å in Fig. 3b). Unlike the Au data in Fig. 2, a second late-time peak of emission is apparent on the first three and last three photodiodes. Figure 3b emphases this effect by comparing the signal recorded by the first 3 diodes with the measured laser pulse shape for the same shot. Results from CH targets illuminated by 3 beams are similar with to those obtained from 10 beams with the exception that the recorded intensities scale approximately with the laser irradiance on target. Radiation from targets made from several other low Z elements ($Z \leq 8$ i.e., BN and Kapton), resembles to a large extent the results from CH targets. Thus in the following we will only mention them in passing.

Plots of the long lasting CH emission in the 1st and 6th channels are plotted in Fig. 4a, the 2nd and 7th in Fig. 4b, and the 3rd and 8th in Fig. 4c. In each plot, the pairs are similar with the exception that the intensities from the three longer wavelength channels (dashed lines) are lower by about a factor of 1.5 and are slightly earlier in time than the shorter wavelength channels (solid lines). The fact that the radiation is detected at photodiodes that are centered on progressively longer wavelengths is a property of the transmission grating spectrometer design and its position relative to the plasma. Earlier studies have shown that laser produced plasmas from planar targets tend to expand primarily along normal to the target surface with little influence from the direction of the incoming laser beam [21]. The results presented in Figs. 2-4 were obtained with the normal to the target surface aligned to the laser beam and the spectrometer line of sight tilted relative to them by ~42°. As indicated in Fig. 1, the laser beam and the Si photodiode array are located on opposite sides of the line of sight. The modest imaging capabilities of the transmission grating spectrometer transfers the expansion of the plasma towards the laser beam along the target normal as a shift of emission towards longer wavelengths at the detector plane.

To demonstrate that the late time radiation resulted from an expanding plasma source, we rotated the normal to the target so it coincided with the spectrometer line of sight and moved the Si photodiode over to observe both sides of zero order. Since the plasma should expand symmetrically around the target normal, the diodes should record late time emission on both sides of zero order. Figure 5a shows the result obtained for a CH target illuminated by 3 beams. The unshifted zero order, which was aligned to appear on the Si photodiode array at a location corresponding to the gap between the 4th and 5th

diodes, was slightly misaligned in the direction of the -1st order. Nevertheless, the late time emission appeared quite symmetrically relative to the zero order.

Finally, to verify further that the observed radiation symmetrically distributed on both sides of the zero order is due to a spatial shift and not to a spectral shift, we realigned the normal to the target to the incoming laser beam, shifted the diodes so they detected radiation on one side of the zero order and replaced the 2500 l/mm grating with a 5000 l/mm grating. If the distribution pattern of the long lasting radiation seen on the first three photodiodes on Fig. 3a was due to wavelength dispersion we would expect that the doubling the dispersion of the spectrometer would cause the radiation to be spread over a larger number of photodiodes in accordance with equation (2). In contrast if the distribution pattern was the result of the source motion, a doubling of the dispersion should cause no change. Figure 5b illustrates the intensity pattern obtained with the 5000 l/mm grating. The fact that it resembles the pattern for the diodes near zero order seen in Fig. 4 confirms that the shift is indeed due to the source motion and not to wavelength dispersion. From the above we conclude that the two patterns of emission, the one that is adjacent to the zero order and to the one adjacent to the position of the C VI Lyα line are the same phenomena seen in two different orders.

Kapton and BN Targets

Experiments with Kapton and BN targets were conducted to verify that the late time signal was typical of the low Z targets. Kapton is a plastic material composed of 56% C, 26% H, 5% N, and 13% O by abundance. Because C atoms dominate, the late emission spectra from Kapton looked similar to the CH spectra. The results from the BN targets were not as clear. The B V Lyα doublet appeared at 48.6 Å and the N VII Lyα

doublet appeared at 24.8 Å. The BN spectra were attenuated either by a 2600 Å thick Ti filter or a 1600 Å thick Al filter. While the Ti filter, which has an absorption edge at ~27 Å, attenuated the intensity of the 24.8 Å N VII Lyα by about a factor of 5 the Al filter attenuated it only slightly. In the case of the B V Lyα (48.6 Å) line the Al filter attenuated the intensity at somewhat larger degree than the Ti filter. The late radiation in channels closest to zero order and in the channels at wavelengths longer than N VII Lyα line was significantly smaller when attenuated by the Ti filter rather than the Al filter. This result indicated that the late-time radiation was predominately from the N VII Lyα line. An inspection of the output of the last photodiode showed some late emission that can be attributed to the B V emission but it seemed to be rather small. For both Kapton and BN we believe that we observed similar late-time emission, but that the increased complexity of the spectra and the particular wavelengths relative to the filters used in the spectrometer made the late time emission less clear than the CH case.

IV.3 Moderate Z target

We used an Al target as a representative of the moderate Z elements. The Al XIII Lyα doublet appears at 7.2 Å producing a signature that almost blends with the zero order. Thus if late emission from the Al target material is present it would be brightest in the first two channels. A close inspection of the signals from the Al target showed only a small indication of the late emission. This result may be due to the fact that only a small amount of the Al atoms in the target reach the hydrogenic stage, and/or a slower expansion rate for the Al plasma.

V. Characteristics of the expanding laser-produced plasmas from CH planar targets irradiated by the Nike laser

The late-time emission from CH targets has been shown in Section IV to expand symmetrically around the target axis and from the target surface outward towards the laser beam. With this interpretation, the lack of secondary pulses in the fourth and fifth diodes in Fig. 3a (with the target normal was aligned parallel to the laser beam) implies that the late time emission is limited in spatial extent with a zero order image followed by the diffracted first order image occurring in the sixth, seventh, and eighth diodes. The fifth diode in this case recorded light from the CVI Lyα transition while the plasma was restricted to a region near the target surface, so we are compelled to hypothesize that the late time emission at the adjacent longer wavelength diodes is from the same transition as the plasma expands outward.

We can study the amplitude and timing of the post laser pulse peaks in the diode signals. From inspection of Fig. 3b, it can be seen that the intensity of each diode is always lower throughout time than its neighbor at shorter wavelength, i.e. closer to the target. The expanding emission appears to have a continuous gradient outward from the target. If the plasma conditions are such that the emission decays slowly during the expansion, then the late time peaks are expected as the collection region of a particular diode is filled by the plasma. After the collection region is filled due to expansion, then the signal would monotonically decay, as observed. The peaks represent the spatial and temporal average of the emission from the propagating 'front' of the expanding plasma.

Figure 6a plots the peak intensities against the time that they occurred from a series of 3 beam shots with the target normal aligned along the laser. The empty symbols

are peaks observed in the longer wavelength diodes and the filled symbols are from the diodes close to zero order. The absolute calibration of the spectrometer's components has been used to estimate the absolute intensity of the emission for each diode with the assumption that the zero order and first order image is dominated by CVI Lyα emission. Although the values show some scatter (probably due to the small variations in laser irradiance among the shots), the two sets of data appear to describe a single curve. A curve fit has been performed to the combined data using a simple functional form:

$$I(t) = I_o \, t^{-\beta} \qquad (5)$$

where t is the time at which the peak is observed for a given diode. The solid line in Fig. 6a represents the results from the fit which yielded $I_o = 1.7 \times 10^7$ Wster^{-1} and $\beta = 3.1$. A t^{-3} time dependence is exactly the one expected if the plasma density, ρ, of a moving source was monitored as it experienced free expansion as $\rho(t) \propto R^{-3}(t) \sim (v\,t)^{-3}$, where v is the expansion velocity.

From the studies of the peaks and the target alignment (see Section IV), we can also investigate the position of the peaks as a function of time. The position of the peaks has been estimated with reference to emission during the main laser pulse. For the zero order image, the laser spot position is the estimated initial position of the plasma. For the diodes from the first order image, the assumption that the peak emission arises from CVI implies that we can use the position of CVI radiation during the pulse as the spatial origin. From the separation of the nth diode center from its reference diode (X~1.07 mm/diode of separation), the magnification of the spectrometer's geometry (~0.57 from Section III), and the angle between the target normal and the spectrometer's line of sight

(θ), the position diode's collection region, ℓ, the laser spot (X=0 mm) can be calculated:

$$\ell = \frac{nX}{0.57\sin(\theta = 42^o)} \qquad (6)$$

for target normal along the laser beam. When the target normal is along the spectrometer's line of sight, the $\sin\theta$ correction is not needed. In the former case, the estimated position is the distance from the target surface along the normal and, in the latter case, the position is the radial distance from the laser spot. Note that the estimated positions will be in the range of 1-10 mm given the relatively large size of the diodes compared to the laser focal spot (~750 μm diameter spot for these experiments). The error in the peak position is given by the spatial resolution estimated in Section III with the additional $1/\sin\theta$ correction as in Eq. 6 for the position along the target normal.

Figure 6b shows the estimated position of each peak versus the time at which the diode recorded the peak emission. As in Fig. 6a, the open data symbols correspond to the long wavelength diodes and the closed symbols represent data from diodes close to zero order. The circles and triangles represent data taken with the target normal aligned to the laser beam (i.e. the estimated expansion parallel to the target normal) and the squares represent data with the target normal aligned along the spectrometer's line of sight (i.e. estimated expansion perpendicular to the target normal). Data taken with the 2600 Å Ti filter installed is represented by the circles and squares and the triangles represent data taken with the 1600 Å Al filter installed.

The data points in Fig. 6b clearly demonstrate two separate groupings: one for the perpendicular expansion and one for the parallel expansion of the plasma. There is limited data available for the perpendicular case due to the fact that the diodes were only aligned to zero order for that target orientation. For the parallel expansion, the zero order and the first order images show fairly consistent results. The data with the Ti filter (the empty and filled circles) may show a slight difference at the late times, but the Al filter data (the empty and filled triangles) do not show such a difference. For the zero order Ti data (the filled circles) there is a significant spread of times near the 9 mm positions compared to the estimated error in the fits used to estimate the time of the peak. More data would be need to determine if there is a significant difference between the first order and zero order observations at large distance. The slight delay noted in Fig. 3b can now be seen to result from the fact that the collection region for the zero order image was centered at a position slightly further from the laser spot than the collection region for the first order image.

The distinction between the two expansion directions can be further quantified as indicated by the linear fits included in Fig. 6b. The fits demonstrate that the parallel expansion occurs at a velocity of 4.7 (+/-0.1) x 10^7 cm/sec and the perpendicular expansion occurs at a velocity of 2.3 (+/-0.1) x 10^7 cm/sec. The expansion is clearly not spherical for the region of observation, but indicates a total cone angle $\Phi \approx 2 \arctan(2.3/4.7) \sim 52^o$. The large ratio of the two velocities implies that a complete description of the expansion is not as simple as a spherical expansion from a point source, despite the apparently large distance over which the plasma has expanded (~20x the laser spot size).

The existence of long lasting emission from Nike targets implies that recombination of the plasma ions occurs slowly compared to the volume expansion of the plasma. Atomic processes relevant to the emission observed from the expanding plasma were identified as radiative recombination, three body recombination, and electron impact excitation and ionization by the early investigatiors of expanding laser-produced plasmas [1-8]. Each of these processes depends on the ion charge state, the ion and electron densities, and the electron temperature. From the FAST code suite developed at NRL [10,22], a relatively high temperature (T_e ~100's of eV), low density (0.01%-0.1% or less of solid density) region exists at large distances from the target (x > 1 mm) near the end of the laser pulse. A simple criterion for the relative importance of radiative recombination over three body recombination can be derived from analytic approximations of each rate for a plasma with ions primarily in charge state, Z:

$$n_e >> \frac{3x10^{13}\, T_e^{3.75}}{Z}\, cm^{-3} \qquad (5)$$

where three body recombination will be more important than radiative recombination if the inequality holds (Z~6 in our case) [5]. From the orders of magnitudes listed above, the criterion is not met, so radiative recombination will dominate in our region of interest. The absolutely calibrated intensity (10^6 –10^7 W/ster) and the estimated collection volume (~10 mm $^{-3}$) can be used to estimate the rate of photon emission in Lyman-α line of hydrogen-like carbon as being on the order of 10^{16} photons cm^{-3} ns^{-1}, assuming isotropic emission into 4π. Because a large fraction of the ions are fully ionized at the end of the laser pulse (i.e. the ion density is on the order of 10^{19} cm^{-3} ~0.1% solid density for x > 1 mm), the observed radiative recombination involves a relatively small fraction of the total

number of ions in the plasma. Hence, the observed intensity decay should be strongly influenced by the volume expansion at the beginning of the post pulse evolution. The subsequent evolution of the recombination rates, however, depends critically on the time evolution of the electron temperature. A theoretical argument with some experimental corroboration has been advanced for a model assuming the adiabatic expansion of an ideal gas [5]. This model predicts the temporal evolution of the electron temperature as $T_e \propto t^{-2}$. This slower decay of the electron temperature would help maintain the low radiative recombination rate observed in this paper, but, for an accurate quantitative treatment of the post-pulse expansion, the details of electron and ion heating by radiation transfer and three-body recombination needs to be considered.

In comparison to the early papers [1-8] this work has measured slightly higher expansion velocities ~5×10^7 cm/sec than were seen in some of the earlier spectroscopic studies where values 3×10^7 cm/sec were seen at lower laser powers (typical on the order of 1 J in ~10 ns then as compared to ~100 J in 4 ns now). More recently [23,24], researchers have conducted studies at similar laser powers but employed charged particle analyzers rather than spectroscopic instruments. While these experiments determined velocities on in the same range as for this work, a notable distinction is that these particle measurements were made at a much larger distance from the target and were capable of extracting information on all of the ion charge states.

Acknowledgements

This work was supported by the U.S. Department of Energy, NNSA-Defense Programs. We acknowledge very informative discussions with Marcel Klapisch. We also thank the Nike laser and target crews (Denis Brown, Laodice Granger, Del Hardesty, Bruce

Jenkins, Steve Krafsig, Nick Nocerino, J. Picciotta, Zeb Smyth, and Steve Terrell) for their efficient, professional effort in operating the laser facility.

References

1. B. C. Boland, F. E. Irons, R. W. P. McWhirter, J. Phys. B **2**, 1180 (1968).

2. H. Puell, Z. Naturforsch **25a**, 1807 (1970).

3. H. Puell, H. J. Neusser, W. Kaiser, Z. Naturforsch **25a**, 1815 (1970).

4. F. E. Irons, R. W. P. McWhirter, N. J. Peacock, J. Phys. B **5**, 1975 (1972).

5. P. T. Rumsby, J.W. M. Paul, Plasma Phys. **16,** 247 (1974).

6. F. E. Irons, N. J. Peacock, J. Phys. B **7**, 2084 (1974).

7. M. Galanti, N. J. Peacock, J. Phys. B **8**, 2427 (1975).

8. F.E. Irons, J. Phys. B **8**, 3044 (1975).

9. S. E. Bodner, D. G. Colombant, J. H. Gardner, R. H. Lehmberg, S. P. Obenschain, L. Phillips, A. J. Schmitt, J. D. Sethian, R. L. McCrory, W. Seka, C. P. Verdon, J. P. Knauer, B.B. Afeyan, H. T. Powell, Phys. Plasmas **5**, 1901 (1998).

10. D. G. Colombant, S. E. Bodner, A.J. Schmitt, M. Klapisch, J. H. Gardner, Y. Aglitskiy, A. V. Deniz, S. P. Obenschain, C. J. Pawley, V. Serlin, J. L. Weaver, Phys. Plasmas **7**, 2046 (2000).

11. T. Kita, T. Harada, N. Nakano, H. Kuroda, Applied Optics, **22,** 512 (1983).

12. R. J. Fonck, A. T. Ramsey, R. V. Yelle, Applied Optics, **21**, 2115 (1982).

13. N. M. Ceglio, R. L., Kauffman, A. M. Hawryluk, H. Medecki, Applied Optics **2**, 318 (1983).

14. M. Chaker, V. Bareau, J. C. Kieffer, H. Pepin, T. W. Johnston, Rev. Sci. Instrum. **60**, 3386 (1989) .

15. T. Wilhein, S. Rehbein, D. Hambach, M. Berglund, L. Rymell, H. M. Hertz, Rev. Sci. Instrum. **70**, 1694 (1999).

16. S. A. Bel'kov, B. A. Bryunetkin, N. V. Zhidkov, I. Yu Skobelev, N. A. Suslov, A. Ya Faenov, Quantum Electronics **24**, 234 (1994).

17. J. L. Bourgade, P. Combis, M. Louis-Jacquet, J. P. Le Breton, J. de Mascureau, D. Naccache, R. Sauneuf, G. Thiell, C. Keane, B. MacGowan, D. Matthews, Rev. Sci. Instrum. **59**, 1840 (1988).

18. K. Eidmann, T. Kishimoto, P. Herrmann, J. Mizui, R. Pakula, R. Sigel, S. Witkowski, Laser and Particle Beams **4**, 521 (1986).

19. J. F. Pelletier, M. Chaker, J. C. Kieffer, J. of X-ray Science and Technology **6,** 359 (1996).

20. J. L. Weaver, U. Feldman, J.F. Seely, G. Holland, M. Klapisch, D.Colombant, A. Mostovych, V. Serlin, Phys. Plasmas **8,** 5230 (2001).

21. G. A. Doschek, U. Feldman, P. G. Burkhalter, T. Finn, W.A. Feibelman, J. Phys. B **10,** L745 (1977).

22. J. H. Gardner, A. J. Schmitt, J. P. Dahlburg et al, Phys. Plasmas **5**, 1935 (1998).

23. G. L. Payne, J. D. Perez, T. E. Sharp, B. A. Watson, J. Appl. Phys. **49,** 4688 (1978).

24. P. D. Gupta, P. A. Naik, H. C. Pant, J. Appl. Phys. **55,** 701 (1984).

Figure Captions

Figure 1: Schematic of experimental setup shows relationship between laser produced plasma and the line of sight for the transmission grating spectrometer. The front module of the spectrometer contains the entrance slit, transmission filter, and transmission grating assembly. The rear module contains the aperture mask, the Si photodiode array, and the CCD array.

Figure 2: Sample time histories of the recorded voltages from the Si photodiode array are shown for a Au foil target illuminated with a laser power density of 1.6×10^{13} W cm $^{-2}$. The abscissa is time with the long dashed vertical line indicating t=0 for each diode. The center wavelength of each diode is noted at the top of the graph. For comparison, the time history of the laser pulse is included after the longest wavelength diode.

Figure 3: Sample time histories from the Si photodiode array are shown in part (a) for a CH target illuminated with a laser power density of 2.2×10^{13} W cm $^{-2}$. Part (b) shows a comparison of the laser pulse shape and the first three photodiode signals from part (a).

Figure 4: A comparison of the late-time signals from Fig. 3a for the 1st and 6th diodes (a), 2nd and 7th diodes (b), and 3rd and 8th diodes (c) shows that the peak emission in each pair occurs at nearly the same time. The signals from the 6 th, 7 th, and 8th diodes are plotted as dashed lines. The wavelengths at the center of each of these diodes were shown in Fig. 3a.

Figure 5: Part (a) shows the diode time histories for emission from a CH target with the spectrometer aligned such that the undispersed light transmitted by the grating (zero order) fell approximately on the middle of the Si photodiode array and the target normal is aligned along the spectrometer line of sight. The late time signal is seen to be approximately symmetric in wavelength. Part (b) shows the observation near zero order when a 5000 l/mm grating was used in the spectrometer. For each diode in both part (a) and (b), a 45 ns long segment of the diode signal is shown.

Figure 6: A quantitative examination of the late time emission peaks is presented. Part (a) plots the time history of the intensities of the peaks for data taken with a 2600 Å Ti filter and the target normal aligned to the laser beam direction. The filled circles represent data from the zero order (short wavelength) diodes and the empty circles represent data from the first order (longer wavelength) diodes. The dotted line is a curve fit that yielded a time dependence of $I \propto t^{-3.1}$. Part (b) shows the time history of the position of the peaks from the various diodes. The solid and empty circles have the same meaning as in (a). The triangles are from experiments with the target normal along the laser beam, but with a 1600 Å Al filter. The filled and empty triangles are from the zero and first order images, respectively. The data represented by filled squares are the peaks observed when the target normal was aligned along the spectrometer line of sight. For this data the 2600 Å Ti filter was used and only zero order diode data was available. The plotted lines represent linear fits to the collected data for each of the two target alignments.

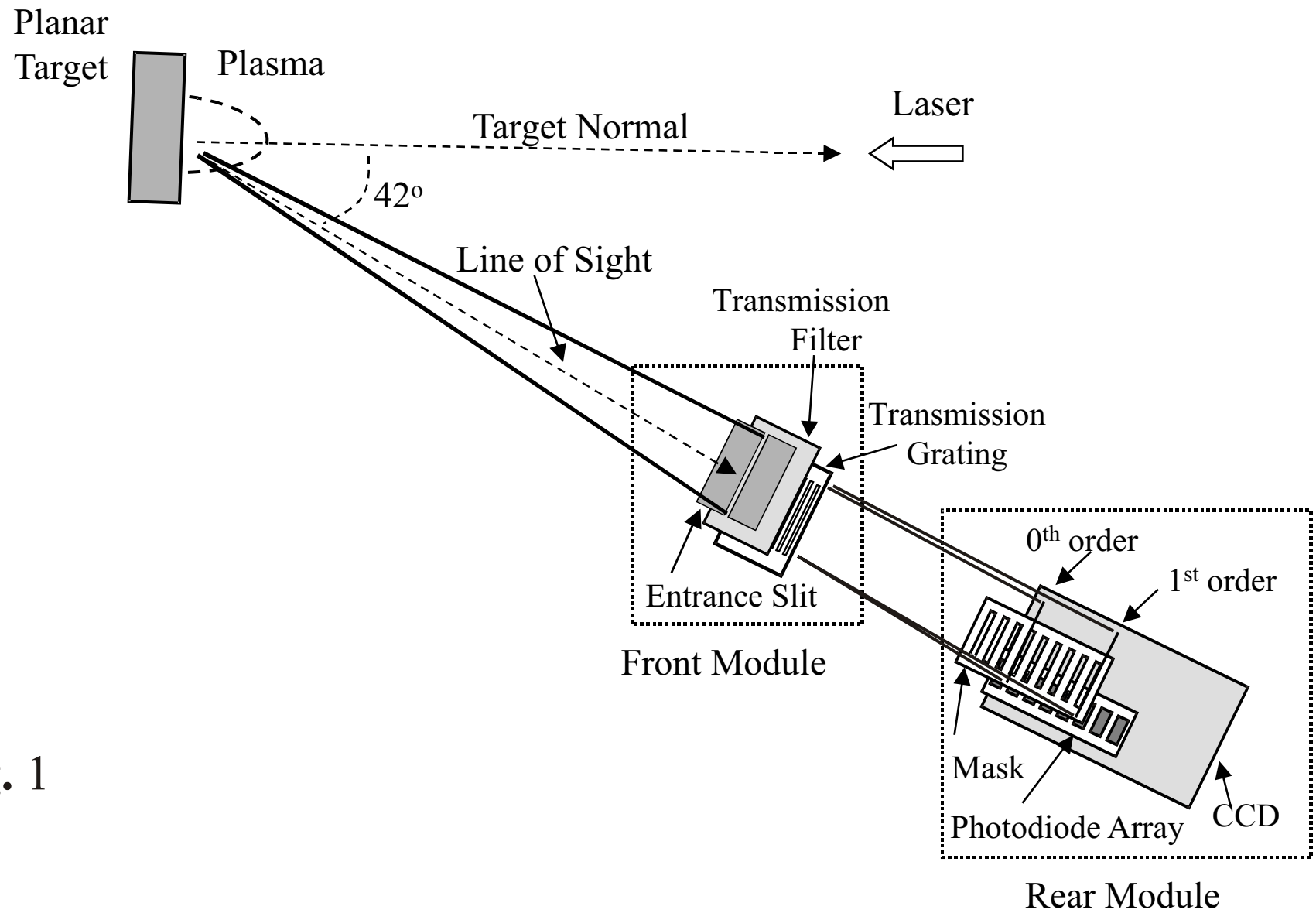
Planar
Target
Plasma
Target Normal
Laser
42°
Line of Sight
Transmission
Filter
Transmission
Grating
Entrance Slit
Front Module
0th order
1st order
Mask
Photodiode Array
CCD
Rear Module

Fig. 1

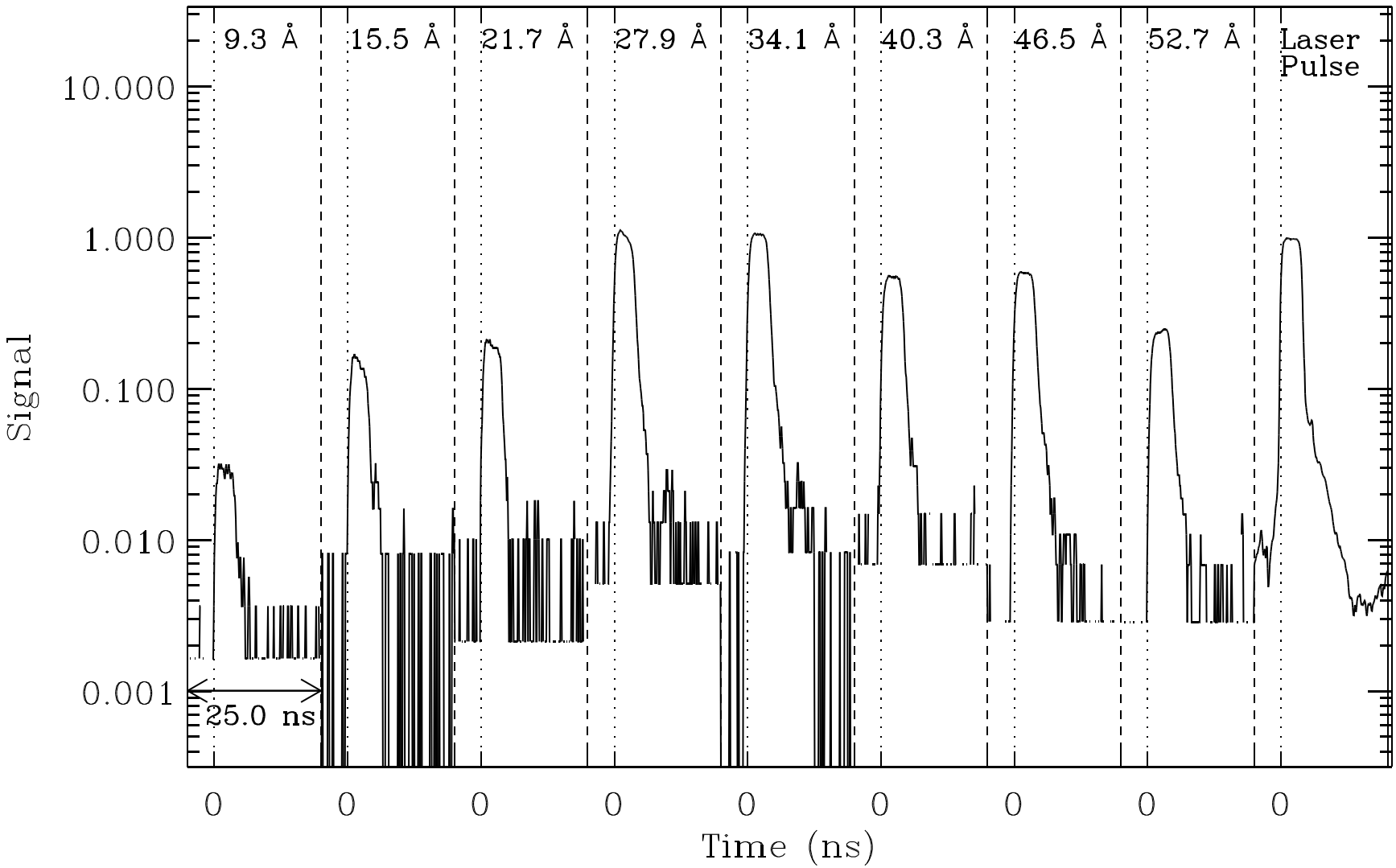
9.3 Å
15.5 Å
21.7 Å
27.9 Å
34.1 Å
40.3 Å
46.5 Å
52.7 Å
Laser Pulse
10.000
1.000
0.100
0.010
0.001
Signal
25.0 ns
0
0
0
0
0
0
0
0
0
Time (ns)

Fig. 2

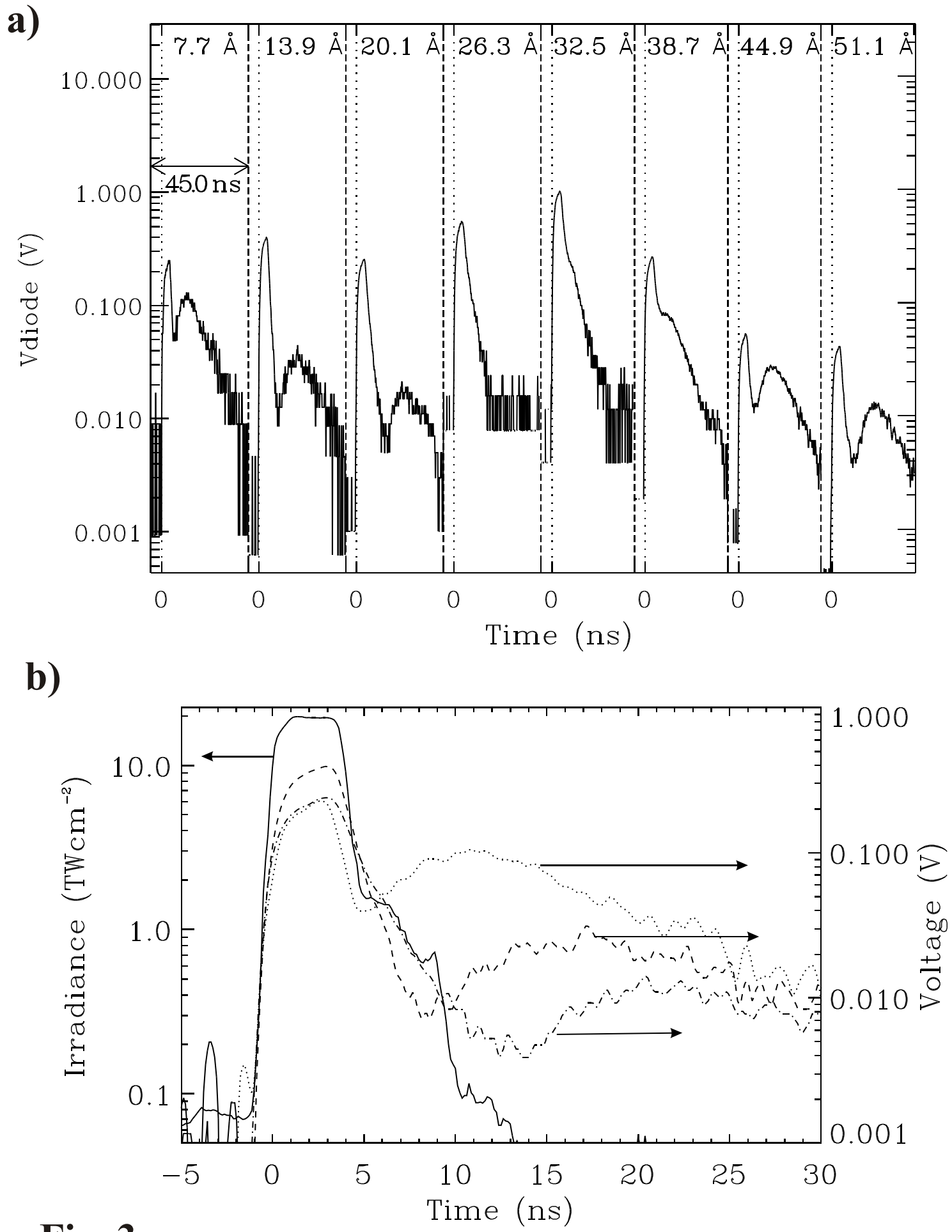
a)
7.7 Å
13.9 Å
20.1 Å
26.3 Å
32.5 Å
38.7 Å
44.9 Å
51.1 Å
45.0 ns
10.000
1.000
0.100
0.010
0.001
Vdiode (V)
0
0
0
0
0
0
0
0
Time (ns)
b)
10.0
1.0
0.1
Irradiance (TWcm^{-2})
1.000
0.100
0.010
0.001
Voltage (V)
−5
0
5
10
15
20
25
30
Time (ns)

Fig. 3

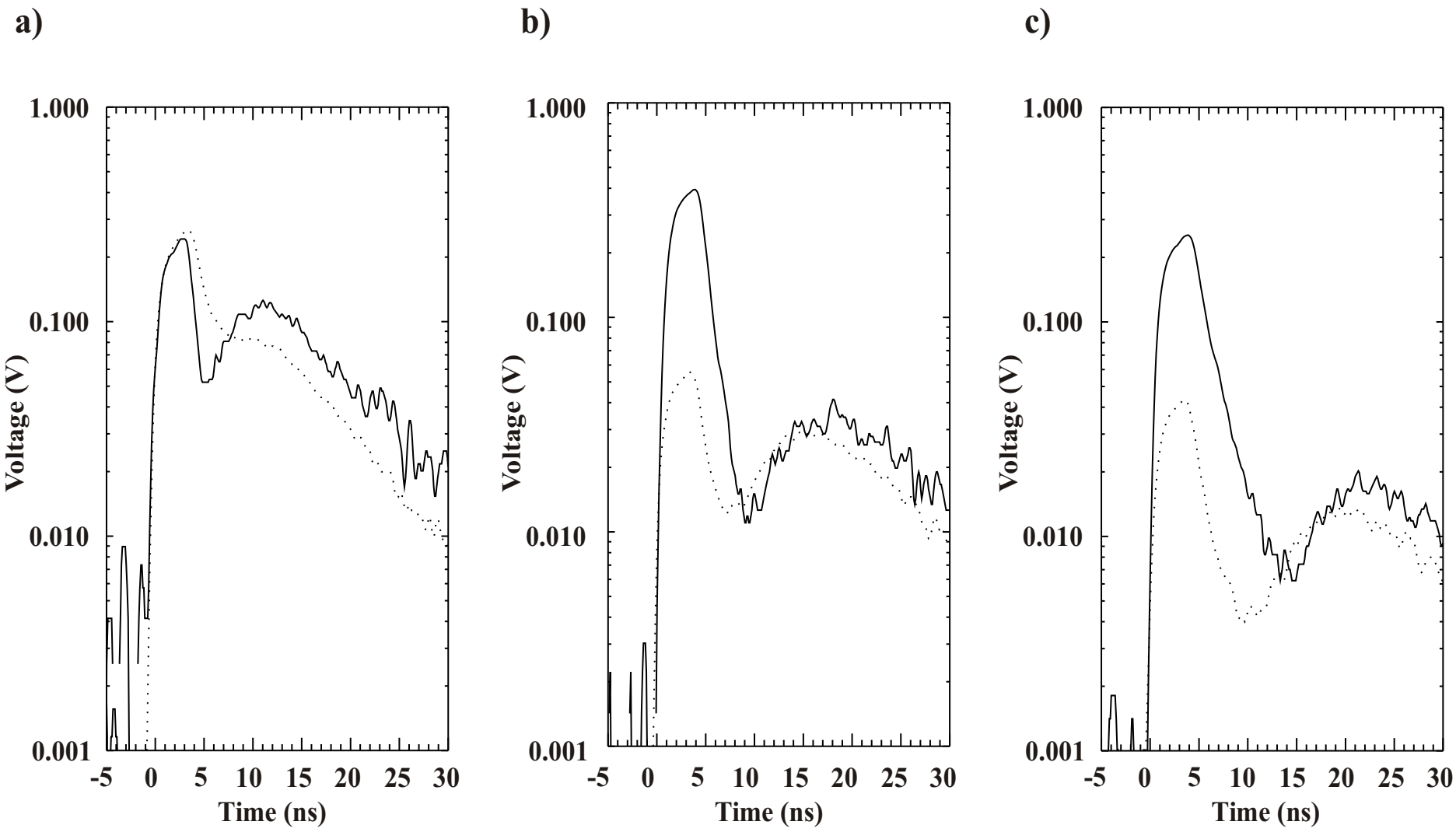

Fig. 4

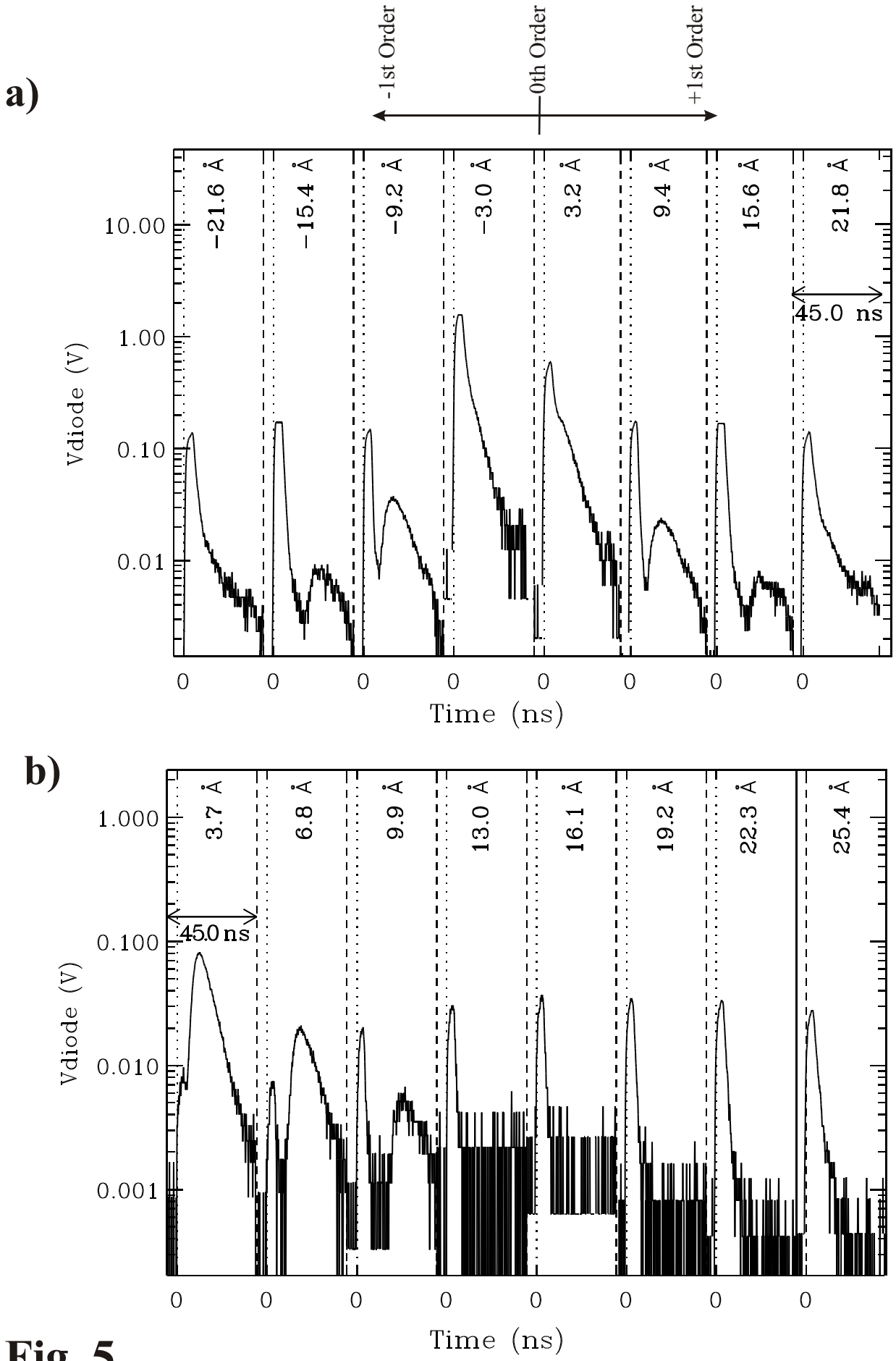
a)
-1st Order
0th Order
+1st Order
−21.6 Å
−15.4 Å
−9.2 Å
−3.0 Å
3.2 Å
9.4 Å
15.6 Å
21.8 Å
45.0 ns
10.00
1.00
0.10
0.01
Vdiode (V)
Time (ns)
b)
3.7 Å
6.8 Å
9.9 Å
13.0 Å
16.1 Å
19.2 Å
22.3 Å
25.4 Å
45.0 ns
1.000
0.100
0.010
0.001
Vdiode (V)
Time (ns)

Fig. 5

a)

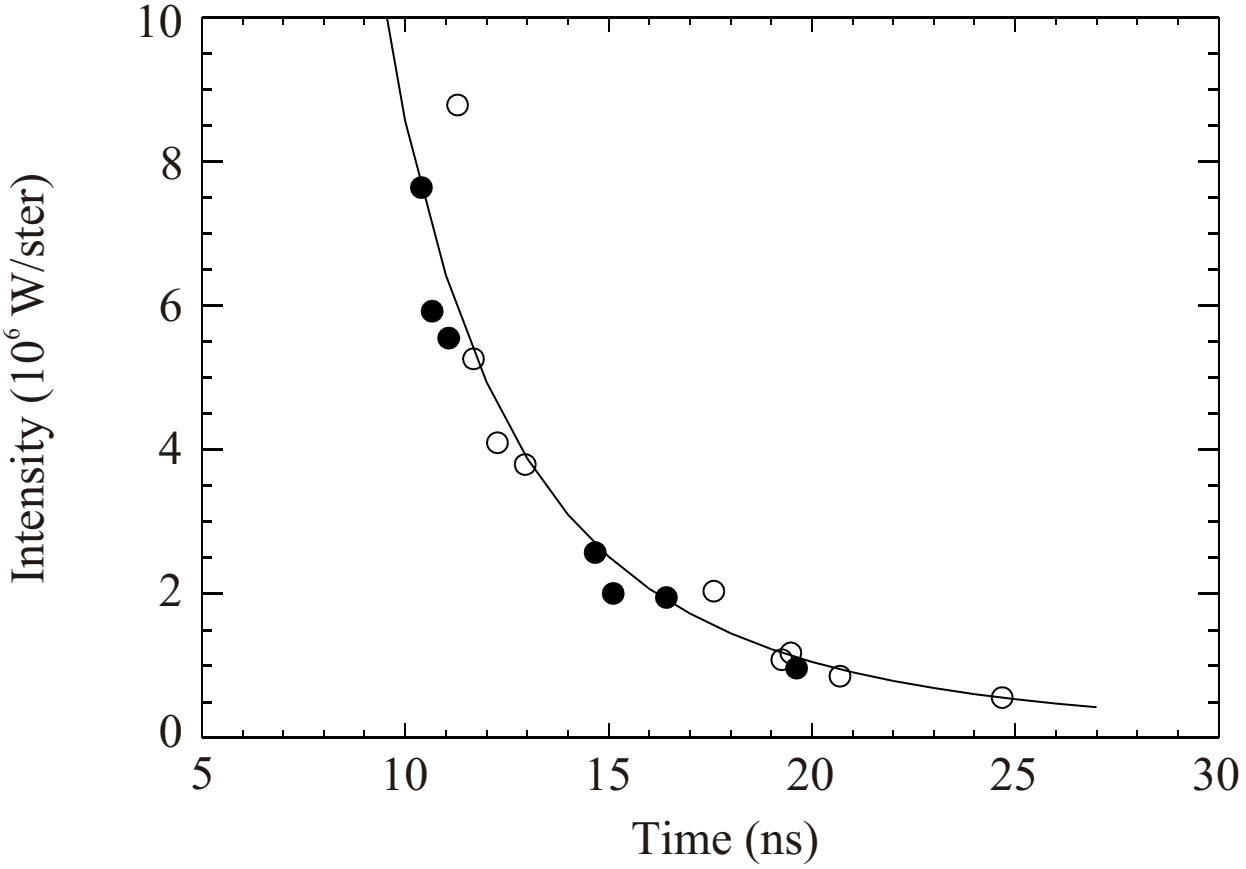
Intensity (10^6 W/ster)
Time (ns)
0
2
4
6
8
10
5
10
15
20
25
30

b)

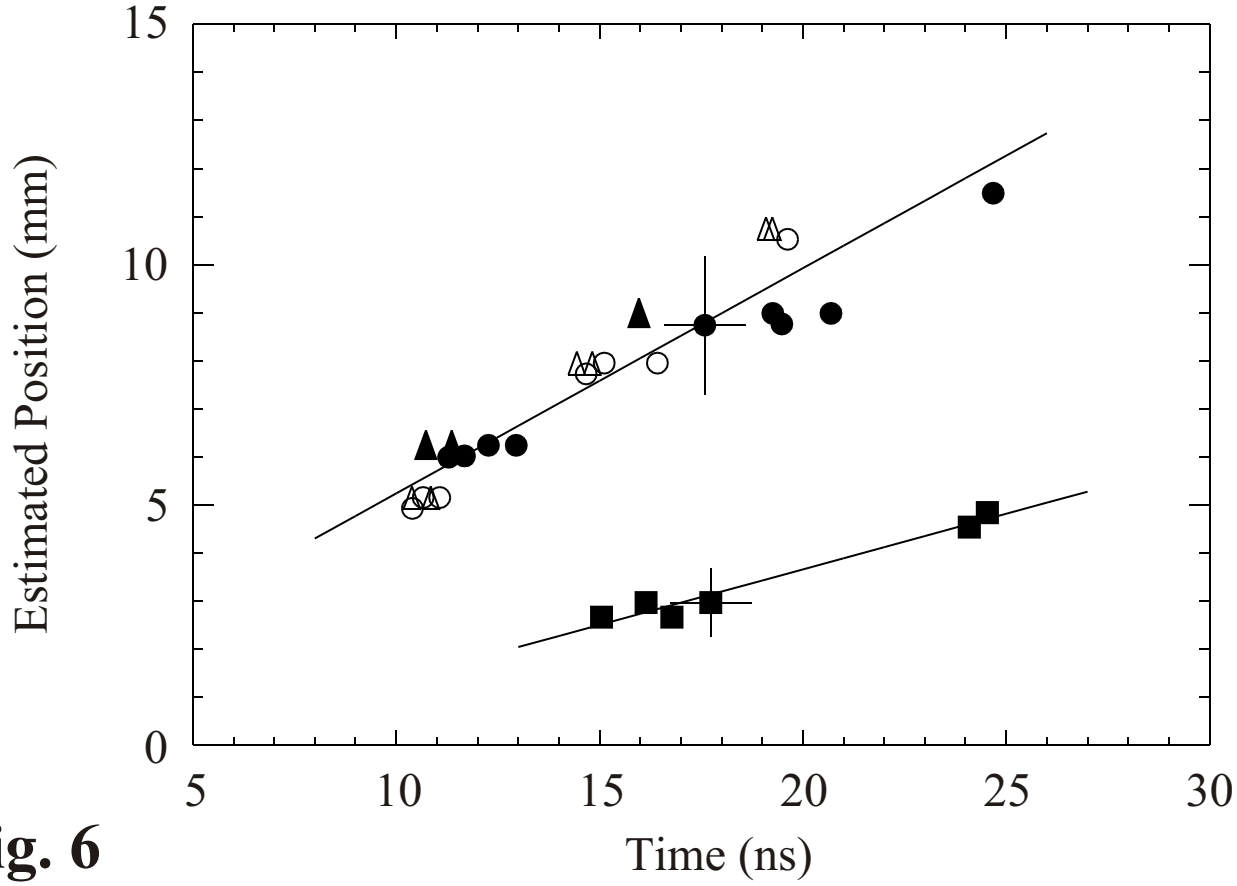
Estimated Position (mm)
Time (ns)
0
5
10
15
5
10
15
20
25
30

Fig. 6